Analytical Prediction of Stability Limit in Turning Operations

E. Ozlu, E. Budak *
Sabanci University, Faculty of Engineering and Natural Sciences, Orhanli, Tuzla 34956, Istanbul, Turkey,
* ebudak@sabanciuniv.edu

Abstract
Unstable cutting due to chatter vibrations is one of the most important problems during metal cutting operations. Chatter can be a limitation for productivity and surface quality in turning operations, especially when long and slender tools and parts are involved. In this study, an analytical stability method for turning process is presented. The model takes the cutting geometry into consideration, and proposes a new solution procedure for the dynamic chip thickness at the insert nose. The analytically calculated absolute stable depth of cuts are compared with the chatter test results, and a good agreement is observed.

1 INTRODUCTION

Instability of cutting processes is an important problem due to resulting high cutting forces, poor surface quality and reduced productivity. Although chatter is a more common problem in milling operations, it can be a limiting factor in some turning operations where slender and flexible tools and parts are involved. The analytical prediction of stability lobes for orthogonal cutting is well established, however only a few attempts have been made for modeling and analysis of turning stability considering the true geometry of the process. This study focuses on the analytical treatment of the process dynamics, and stability predictions in turning operations.

The mechanics of instability in cutting processes was first understood by Tlusty [1] and Tobias [2]. They observed that the modulated chip thickness due to vibrations affect cutting forces dynamically, which in return increases vibration amplitudes yielding a process named as the regenerative chatter. They also observed that the depth of cut was the key process parameter in the cutting process stability. Tlusty [1] analytically showed that for the depth of cuts higher than the stability limit, the magnitude of the dynamic forces and oscillations increases yielding instability, thus chatter vibrations. In his orthogonal stability model, Tlusty [1] used an oriented model resolving cutting forces and structural dynamics into one direction, i.e. the chip thickness direction, reducing the dynamic problem into a 1-dimensional (1D) case. Although this is a valid model for a truly 1D operation such as plunge turning or straight turning without side-cutting-edge angle and nose radius, it is not an accurate model for many cases where multi dimensional cutting and/or dynamics are involved. This is similar to the case of vibration analysis of 2 degree-of-freedom (DOF) system. This system has 2 natural modes which can be determined by a simple 2D eigenvalue analysis. Lumping or resolving the system parameters in one direction would result in a 1D system, and one natural mode which is different than any one of the two actual natural frequencies. Thus, reducing the true dynamic order of the system results in erroneous predictions. Similarly, in dynamic cutting process analysis, reducing a 2D or multi-D cutting system, which can only be accurately represented as an eigenvalue problem, into a single algebraic equation would result in inaccurate stability predictions. This has been demonstrated in the analysis of milling stability by Minis and Yanushevsky [3] and Budak and Altintas [4]. Later, Rao et al. [5] used Budak's multi directional approach [6] to model the stability in turning, and calculated the dynamic chip area with a cross coupling term, which includes the effect of vibrations in one direction on the chip area in the other direction. Clancy et al.[7] added wear and process damping modeling to the study above. However, in these studies cross coupling term made the modeling complicated. Atabey et al.[8] and Lazoglu et al. [9] proposed an analytical model for force prediction in boring, and using time domain solutions they predicted workpiece topography as well. Ozdoganlar and Endres [10] presented an analytical chip-area representation for corner-radiused tools under both depth-of-cut and feed variation with a precise but complicated model. The studies summarized above (except [7]) solved the stability equations in time domain, i.e. numerically.

In this paper, an analytical model for prediction of stability limits in turning is proposed. The model includes all important parameters of turning geometry, i.e. cutting angles and tool nose radius, in addition to the tool and workpiece dynamics. The model proposed is a step ahead from the previous studies as it includes dynamics of cutter and workpiece in multi directional form (not oriented in one direction), an accurate but practical modeling of tool nose radius and dynamic chip thickness, and a stability limit solution in frequency domain rather than time domain simulations.

The paper is organized as follows. First, the dynamic cutting model is presented where the stability solution procedure is also formulated. This procedure is then modified and adapted to include the insert nose radius as well. The simulations are followed by experimental results and conclusions.

2 ANALYTICAL MODEL

In order to study the stability of turning processes, first the dynamic chip thickness and cutting forces are modeled. Then, the derived dynamic equations are solved as an eigenvalue problem to obtain the stability limits. The chip thickness, *h*, and cutting angles in turning can be seen in Fig.1, where α is the normal rake angle, and *i* and *c* are the inclination and side edge cutting angles, respectively, both measured on the rake face.

2.1 Dynamic Chip Thickness and Forces

In order to formulate the relationship between dynamic turning forces and dynamic chip thickness, all components of the dynamic problem are transformed into the global coordinate system (lathe axes; *x*, *y*, and *z*) which can be seen in Figure 1.b. Observing Figure 1.a and 1.b one can deduce that the dynamic displacements at cutting (*z*) direction do not affect the dynamic chip thickness. By this observation, the dynamic problem is reduced to a 2D model. The modulated chip thickness resulting from vibrations of the tool and workpiece can be written as follows;

$$h_m(t) = f\cos c + \left(x_c^1 + x_w^1 - x_c^0 - x_w^0\right)\cos c + \left(-y_c^1 - y_w^1 + y_c^0 + y_w^0\right)\sin c \qquad (1)$$

where, *f* represents the feed per revolution, (x_c^1, x_w^1) and (y_c^1, y_w^1) are the cutter and workpiece dynamic displacements for the current pass, respectively, and (x_c^0, x_w^0) and (y_c^0, y_w^0) are the cutter and workpiece dynamic displacements for the previous pass in *x* and *y* directions, respectively. The feed term in eqn. 1 represents the static part of the chip thickness. Since the static chip thickness does not contribute to regeneration mechanism, it can be ignored for the purpose of stability analysis. Therefore, the dynamic chip thickness in turning can be defined as follows;

$$h(t) = \Delta x\cos c - \Delta y\sin c \qquad (2)$$

where

$$\Delta x = x_c^1 + x_w^1 - x_c^0 - x_w^0$$
$$\Delta y = y_c^1 + y_w^1 - y_c^0 - y_w^0 \qquad (3)$$

τ is the delay term which is equal to one spindle revolution period in seconds.

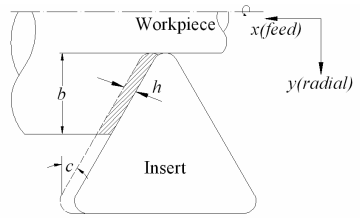

(a)

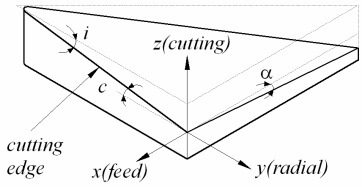

(b)

Figure 1: (a) Chip thickness in turning, b) 3D view of the three cutting angles on the insert.

Although the dynamic problem can be considered as 2D, the cutting process is 3D due to the existence of the inclination angle. Then, the forces at the cutting edge need to be modeled by an oblique cutting model [11].The total force acting on the cutting edge is divided into three components: one parallel to the cutting velocity direction, F_t, one perpendicular to the plane formed by the cutting velocity or F_t and the cutting edge, F_f, and the last one perpendicular to the other two, F_r, (Figure 2).The dynamic cutting forces on the tool can be expressed using eqn.2 as follows;

$$\begin{Bmatrix} F_f \\ F_r \end{Bmatrix} = \frac{b}{\cos c}\begin{bmatrix} K_f \\ K_r \end{bmatrix}\begin{bmatrix} \cos c & -\sin c \end{bmatrix}\begin{Bmatrix} \Delta x \\ \Delta y \end{Bmatrix} \qquad (4)$$

where, K_f, and K_r are the corresponding cutting force coefficients and *b* is the depth of cut (Figure 1.a). Note that F_t is not included in the formulation as it does not take part in the regeneration mechanism. However, it is affected by

the regeneration, and if needed it can be determined using the value of the dynamic chip thickness and the force coefficient in the cutting speed direction, K_t. These coefficients can be directly obtained from calibration tests, or by using the method proposed by Armarego et al.[12] and Budak et al. [13]. In the latter approach, the cutting data obtained in orthogonal tests are used to determine the force coefficients using an oblique transformation, and thus they include the effects of inclination and rake angles.

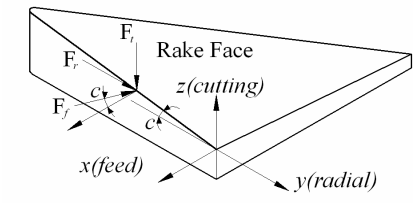

Figure 2: Three components of the total cutting force acting on the insert.

By coordinate transformation the cutting forces can be written in the lathe coordinates as follows:

$$\begin{Bmatrix} F_x \\ F_y \end{Bmatrix} = \begin{bmatrix} \cos c & \sin c \\ -\sin c & \cos c \end{bmatrix} \begin{Bmatrix} -F_f \\ F_r \end{Bmatrix} \tag{5}$$

where, F_x and F_y are the cutting force components in x and y directions, respectively. Substituting eqn. 5 into eqn. 4 we obtain the following relationship;

$$\{F\} = b[A]\{\Delta d\} \tag{6}$$

where $\{F\}$is the force vector and $\{\Delta d\}$ is the dynamic displacement vector both defined in the machine coordinates. The directional coefficients matrix can be expressed as:

$$[A] = \begin{bmatrix} -\cos c & \sin c \\ \sin c & \cos c \end{bmatrix} \begin{bmatrix} K_f \\ K_r \end{bmatrix} \begin{bmatrix} 1 & -\tan c \end{bmatrix} \tag{7}$$

The relationship between the dynamic cutting forces and dynamic chip thickness are given by eqn. 6.

2.2 Chatter Stability Limit

For the stability analysis of the dynamic turning process, a procedure similar to the one used by Budak and Altintas [4, 15] for the milling stability is followed. The response of the cutter and the workpiece at the chatter frequency, ω_c can be expressed as follows;

$$\{d_j(i\omega_c)\} = [G_j(i\omega_c)]\{F\}e^{i\omega_c t} \qquad j = c, w \tag{8}$$

where *{F}* represents the dynamic milling force and the transfer function matrix is given as,

$$[G_j] = \begin{bmatrix} G_{j_{xx}} & G_{j_{xy}} \\ G_{j_{yx}} & G_{j_{yy}} \end{bmatrix} \qquad j = c, w \tag{9}$$

where G_{jxx} and G_{jyy} are the transfer functions in x and y directions ,respectively, and G_{jxy} and G_{jyx} are the cross transfer functions. The vibrations in the previous pass, at time $(t-\tau)$ can be defined as follows;

$$\{d_j^0\} = e^{-i\omega_c\tau}\{d(i\omega_c)\} \qquad j = c, w \tag{10}$$

By substituting eqn. 8 into eqn. 6, we obtain

$$\{F\}e^{i\omega_c\tau} = b(1 - e^{-i\omega_c\tau})[A][G(i\omega_c)]\{F\}e^{i\omega_c\tau} \tag{11}$$

The geometry of tool and workpiece in most of the turning operations are symmetrical and beam like structures, thus for many cases the cross transfer functions are negligible. Then, the transfer matrix can be further simplified as follows:

$$G(i\omega_c) = G_c(i\omega_c) + G_w(i\omega_c) = \begin{bmatrix} G_{xx} & 0 \\ 0 & G_{yy} \end{bmatrix} \tag{12}$$

where, G_{xx} and G_{yy} are the systems total transfer functions in x and y directions. Eqn.11 has a non-trivial solution if and only if its determinant is zero,

$$\det[[I] + \Lambda[G_0(i\omega_c)]] = 0 \tag{13}$$

where, $[G_0(i\omega_c)] = [A][G(i\omega_c)]$, and the eigenvalue Λ is given as,

$$\Lambda = b(e^{-i\omega_c\tau} - 1) \tag{14}$$

The solution of eqn. 13 results in the following:

$$\Lambda = 1/[G_{yy}(K_f \sin^2 c \cos c + K_r \sin c \cos^2 c) + \\ + G_{xx}(K_f \cos^3 c - K_r \cos^2 c)] \tag{15}$$

From eqn. 14, on the other hand, the stability limit, b_{lim}, at a certain chatter frequency can be obtained as follows;

$$b_{\lim} = \frac{\Lambda_R + i\Lambda_I}{\cos\omega_c\tau - i\sin\omega_c\tau - 1} \tag{16}$$

Since b is a real number, the imaginary part of eqn. 16 has to vanish yielding,

$$b_{\lim} = -\frac{1}{2}\Lambda_R(1 + \kappa^2) \tag{17}$$

where,

$$\kappa = \frac{\Lambda_I}{\Lambda_R} = \frac{\sin\omega_c\tau}{1 - \cos\omega_c\tau} \tag{18}$$

Eqn. 18 can be used to obtain a relation between the chatter frequency and the spindle speed [4, 14, 15]:

$$\varepsilon = \pi - 2\psi\ ,\ \psi = \tan^{-1}\kappa \tag{19}$$

$$\omega_c \tau = \varepsilon + 2k\pi\ ,\ n = 60/\tau \tag{20}$$

where, ε is the phase difference between the inner and outer modulations, k is an integer corresponding to the number of waves in a period, and n is the spindle speed in rpm.

The stable depth of cut of the system can be obtained from by eqn. 17 for different chatter frequencies. These frequencies can be searched around the natural frequency of the most flexible structural mode of the system. Then, the corresponding spindle speeds can be determined from eqn. 20 for different lobes, i.e. for *k=1,2,3*…etc. Thus, the stability diagram of the dynamic system can be obtained by plotting the stable depth of cut vs. the corresponding spindle speeds for different lobes [4].

3 MODELING OF THE DYNAMIC CHIP THICKNESS AT THE INSERT NOSE

In the foregoing analysis, the chip thickness and the forces on the straight cutting edge are considered only. In practice, however, turning processes are conducted using cutting inserts with nose radii varying from 0.1 mm to as large as 7-8 mm for better finished surface and cutting performance. For stability analysis, when the (stable depth of cut /nose radius) ratio increases, the importance of including nose radius in the model increases as well. In this study, the chip area at the nose of the tool and at the straight edge is divided into many elements in modeling of the dynamic chip thickness. The chip area in the nose region is divided into n trapezoids as shown in Figure 3. The parameters below are used to describe the chip thickness for each element up to element n.

$$b_e = b_{nose}/n\ ,\ \ b_{nose} = r - r\sin c \quad i=1,...,n \tag{21}$$

$$b_{di} = b_e/\cos\theta_i \quad i=1,...,n \tag{22}$$

$$\theta_i = \frac{\pi}{2} - \tan^{-1}\left(\frac{r - r\sin c}{n s_i}\right) \quad i=1,...,n \tag{23}$$

$$s_i = \sqrt{r^2 - \left(r - \frac{i}{n}(r - r\sin c)\right)^2} - \sum_{j=1}^{i-1} s_j \tag{24}$$

where b_e is the element height or elemental depth of cut, b_{di} is the edge length of the trapezoid, r is the nose radius and θ_i is the angle that defines the orientation of an element edge. By using θ_i, the dynamic chip thickness for the jth element can be defined as follows;

$$h_j(t) = \Delta x\cos\theta_j - \Delta y\sin\theta_j \tag{25}$$

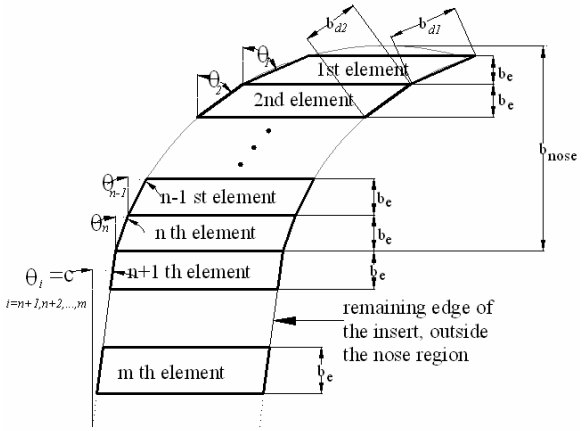

Figure 3: Division of chip thickness by trapezoidal elements.

In this model, *n+1*st element and the following elements up to element *m* are located at the straight cutting edge of the insert; therefore eqn. 21 and 22 is also valid for these elements. But, as it can be seen from Figure 3, their angular orientations are equal to the side edge cutting angle:

$$\theta_i = c \qquad i=n+1,n+2,\ldots,m \tag{26}$$

3.1 Procedure for Solution of Stability Limit with Elemental Nose Model

The nose radius alters the dynamic effects of tool and workpiece on the stability limit by changing the contributions of the tool and workpiece transfer functions on the process dynamics, similar to the effect of side cutting edge angle. Therefore, the dynamic displacements and dynamic forces acting on all elements must be considered in the solution.

Assuming m number of element are in the cut, elemental dynamic forces acting on each element that is in cut can be written from eqn. 6 as follows;

$$\begin{Bmatrix} F_{jx} \\ F_{jy} \end{Bmatrix} = b_e \left[A_j\right] \begin{Bmatrix} \Delta x \\ \Delta y \end{Bmatrix} \quad j=1,2,\ldots,m \tag{27}$$

where, $[A_j]$'s are the directional coefficients that are defined by eqns. 7 and 23. Note that in eqn. 27 the dynamic displacements Δx and Δy represent the total dynamic displacement of the insert in cut, and can be defined as follows,

$$\begin{Bmatrix} \Delta x \\ \Delta y \end{Bmatrix} = \left(1 - e^{-i\omega_c \tau}\right)\left[G(i\omega_c)\right] \sum_{p=1}^{m} \begin{Bmatrix} F_{px} \\ F_{py} \end{Bmatrix} \tag{28}$$

Thus, the dynamic elemental forces can be written by substituting eqn. 28 into 27 as follows:

$$\begin{Bmatrix} F_{jx} \\ F_{jy} \end{Bmatrix} e^{i\omega_c \tau} = b_e \left(1 - e^{-i\omega_c \tau}\right) [A_j] \times [G(i\omega_c)] \sum_{p=1}^{m} \begin{Bmatrix} F_{px} \\ F_{py} \end{Bmatrix} e^{i\omega_c \tau} \quad (29)$$

where, j=1,2,…m. Finally, the total depth of cut of the insert can be calculated as $b=mxb_e$.

Since the dynamic system has now *m* number of degrees of freedom, it can only be solved accurately by a simultaneous solution. Therefore, as Budak et al. [4] applied it for milling stability, it is proposed to merge the dynamic equations into a matrix form which will then be reduced to an eigenvalue problem:

$$\begin{Bmatrix} [F_{1s}] \\ \vdots \\ [F_{ms}] \end{Bmatrix} e^{i\omega_c \tau} = b_e \left(1 - e^{-i\omega_c \tau}\right) [G_0] \begin{Bmatrix} [F_{1s}] \\ \vdots \\ [F_{ms}] \end{Bmatrix} e^{i\omega_c \tau} \quad (30)$$

where, *s=x, y*. $[G_0]$ can be considered as the elemental oriented transfer function and defined as follows:

$$[G_0] = \underbrace{\begin{bmatrix} [A_1] & [A_1] & \dots & [A_1] \\ \vdots & & & \vdots \\ [A_m] & [A_m] & \dots & [A_m] \end{bmatrix}}_{(2m \times 2m)} \underbrace{\begin{bmatrix} [G] & 0 & 0 \\ 0 & \ddots & 0 \\ 0 & 0 & [G] \end{bmatrix}}_{(2m \times 2m)}$$

and the solution is possible if and only if the determinant of eqn. 30 is equal to zero. The eigenvalue Λ is defined as follows.

$$\Lambda = b_e \left(1 - e^{-i\omega_c \tau}\right) \quad (31)$$

As a result of eqn. 31 and 30, the dynamic problem is reduced to the same eigenvalue problem as discussed in section 2.2. Thus, in order to solve the chatter stability limit the same procedure can be followed.

One can notice from eqn. 30 that the solution provides the elemental stability limit, b_{elim}, which is the stability limit for only one element. However the stability limit for the whole system, b_{lim}, is needed to determine the stability limit for all elements that are in the cut. This limit, can be determined by multiplying the elemental stability limit with the number of elements, i.e. $b_{lim}=mxb_{elim}$. This creates one more unknown, *m*, for eqn. 30. Moreover, b_{lim} should be smaller than the total depth of cut of all elements in cut, *b*. In order to calculate *b*, b_e is needed which brings a second unknown. In order to overcome the difficulty created by these two unknowns, an iterative procedure is proposed. The main idea of the iteration is to guess *m* and b_e at the beginning, and check whether b_{lim} is smaller than *b*. If b_{lim} is found to be grater than *b*, then the iteration continues by increasing *m* or decreasing b_e at the next step. It should be noted here that, selecting bigger m values or smaller b_e values increases the precision of the solution. Once the stability limit for the system is found, stability diagrams can be constructed with the method discussed at section 2.2.

The main difference of this procedure from the method given in section 2.2 is the way the eigenvalue is solved. In one element solution the eigenvalue can be calculated analytically. However, for the multi-element model, as the number of elements increases, so does dimension of the directional coefficient matrix. Therefore, a numerical solution is needed for the eigenvalue of the dynamic system.

4 SIMULATION RESULTS

The stability formulation explained in the previous sections has been formulated in order to perform simulations, and to illustrate the effects of different parameters on turning stability. Some of the simulation results will be given in this section. The common values used in the simulations are listed in Table 1.

Table 1: Common values used in the simulations.

Rake angle, α	5°
Inclination angle, *i*	5°
Structural damping coefficient	%0.6
Natural frequencies of tool&w.p	1200 Hz
Shear Stress at shear plane	600 MPa
Friction angle	28°
Shear angle	30°

4.1 Effect of Tool and Workpiece Stiffness and Side Cutting Edge Angle on the Stability Limit

In order to observe the effect of tool and workpiece stiffness and the side cutting angle on the absolute stable depth of cut, the proposed stability model is used for an insert without nose radius, for three different side edge cutting angles, c=10°, 30°, and 45°. The stiffness values used are summarized in Table 2, and the other common data are listed in Table 1. The simulation results can be seen in Figure 5. For higher tool stiffness values (left hand side of Figure 5) the absolute stable depth of cut is more sensitive to the side edge cutting angle, *c*. This is because of the fact that the angle *c* increases the effect of workpiece (which is more flexible)

Table 2: The stiffness value trend used in simulations.

k_ratio	k_w (N/mm)	k_t (N/mm)
0.1	$5x10^4$	$50x10^4$
1	$5x10^4$	$5x10^4$
10	$50x10^4$	$5x10^4$

dynamics on the chip thickness decreasing absolute stability limit. However, as the stiffness of the tool decreases, higher side edge cutting angles increases the effect of workpiece (which is more rigid this time) dynamics on the stability, increasing absolute stability limit. As for the high workpiece rigidity case the effect of workpiece dynamics on the stability is minimal, the process is less sensitive to side edge cutting angle.

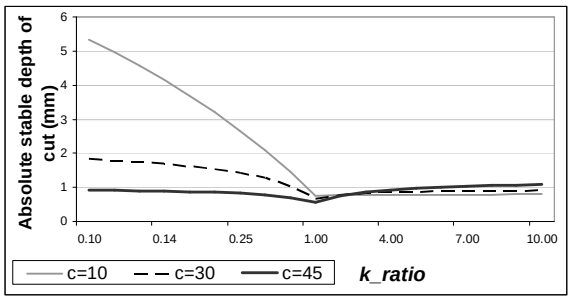

Figure 5: Variation of b_{abs} with tool and workpiece stiffness for different *c* values.

4.2 Effect of Insert Nose Radius

In order to analyze the effect of insert nose radius on the absolute stable depth of cut, simulations are conducted with three different nose radii, *r*=0.4, 0.8 and 1.2 mm, for different tool and workpiece stiffness values listed in (Table 2). The side edge cutting angle used in these simulations is 0°.

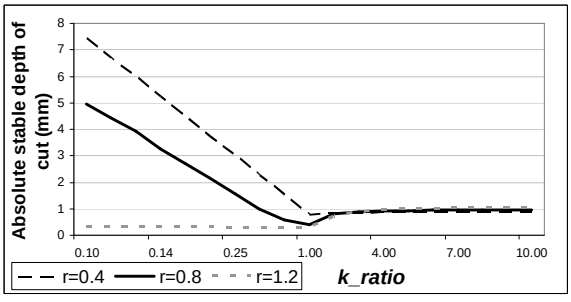

Figure 6: Variation of b_{abs} with tool and workpiece stiffness for different *r* values.

The simulation results can be seen in Figure 6. As discussed at section 3.1 the nose radius affects the stability in the same way as the side edge cutting angle does. This can also be observed from the similarity of Figures 5 and 6. On the left hand side of Figure 6, where workpiece is more flexible, increase in nose radius increases the contribution of workpiece dynamics to the stability resulting in reduction of the absolute stability limit. On the right hand side of Figure 6, where the tool is more flexible, since the dynamics of the system is mainly controlled by the tool the effect of nose radius is low. However, an expected trend is noticeable where the increase in nose radius increases the contribution of workpiece dynamics, which is more rigid in this case, into stability increasing absolute stable depth of cut.

5 EXPERIMENTS

In order to verify the presented analytical stability model, an experimental setup was prepared. It should be noted again that the main objective of the experiments was to verify the absolute stability limit.

5.1 Experimental Setup

A manual lathe is used in tests. Since the gear ratios of the lathe allow only for specific spindle speeds, the tests were conducted at 1000, 1400, and 2000 rpm's. In all of the tests the tool was much more flexible compared the workpiece. In order to obtain the Frequency Response Functions (FRF) of the cutter and workpiece, a modal test setup, and to measure the chatter frequency a microphone data acquisition setup is used (Figure 7.a and 7.b).

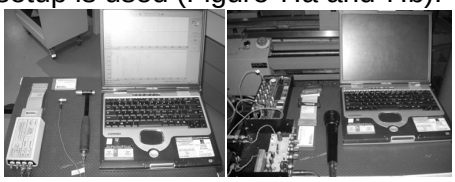

(a) (b)

Figure 7: (a) Modal test setup with CutPro ® [16], (b) Frequency measurement setup.

The workpiece material used during the tests is a medium carbon steel (AISI 1040), and zero rake carbide inserts are used as cutting tools (Figure 8.a, 8.b, and 8.c). The rake and inclination angles can be varied by using different inserts and/or tool holders. However, to avoid eccentricity and to cover a wider ranges of angles in a practical manner, insert seats with different angles were ground and used under the inserts during the cutting tests (Figure 8.d and 8.e).

(a) (b) (c) (d) (e)

Figure 8: Triangular inserts used during tests with radiuses (a)0.4 mm, (b)0.8 mm, (c)1.2 mm. Ments, (d) Regular insert seat, (e) Ground insert seat for desired rake and inclination.

Side edge cutting angle is varied by rotating the tool holder from its clamped end. All of the tests were conducted using a feed rate of 0.08 mm/rev. An existing orthogonal cutting database was used for the prediction of cutting coefficients.

5.2 Experiment Results

5.2.1 Verification of the analytical model

The cutting angles and geometry used in the tests are listed in Table 3. All the other parameters that are used during verification tests are summarized in section 5.1.

Table 3: Cutting geometry used in verification tests.

Side edge cutting angle	10°
Rake angle	5°
Inclination angle	5°
Insert nose radius	0.4mm

The measured tool and workpiece transfer functions prior to the tests, can be seen in Figure 9, where workpiece is rigidly clamped and tool is much more flexible.

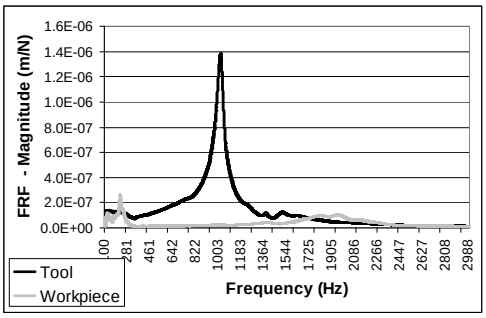

Figure 9: Measured transfer functions of workpiece and tool.

Figure 10 shows the comparison of analytical solution and experimental results. The depth of cuts tested during chatter experiments are selected in order to verify the stable and unstable cut zones, and absolute stability limit. Stable cut zones are tested using depth of cuts fairly under the predicted absolute stability limit. Similarly, unstable cut zones are tested using depth of cuts above the absolute stability limit. In order to confirm the absolute stability limit prediction, a close enough value is selected. In the cutting tests, one direct way of understanding whether there is chatter or not is to observe the finish surface. An example of a finished surface of stable and unstable cut for the tests conducted in 2000 rpm can be seen in Figure 10. Another method to identify an unstable cut is to determine the frequency of the chatter sound. In Figure 11 an example of an FFT measurement can be found for the same test

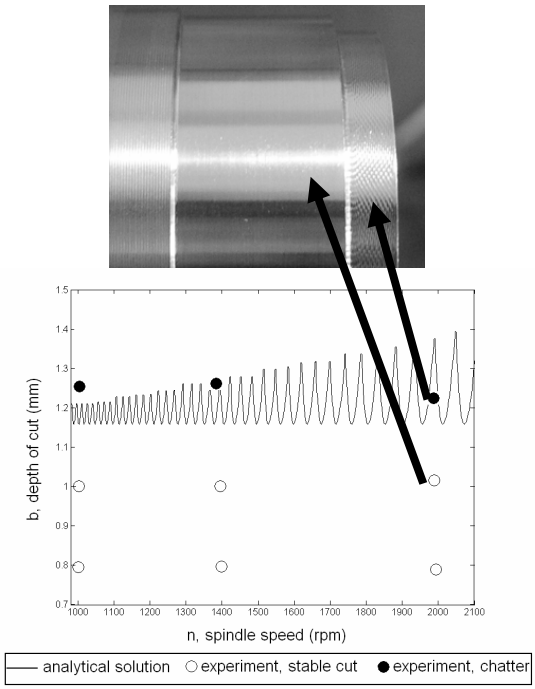

Figure 10: Chatter test results and the cut surface of a stable vs. unstable cut.

at 2000 rpm. The chatter frequency can be clearly seen, which was measured to be about 1000 Hz at unstable depths of cuts close to stability limit, as expected from the transfer function (Figure 9). It can be concluded from these test results that the analytical model can successfully predict the chatter limit.

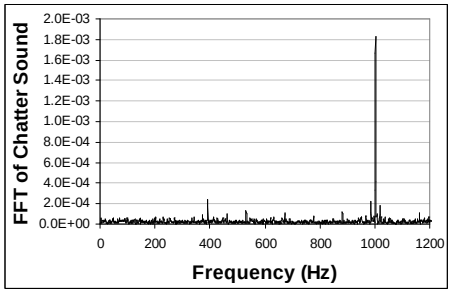

Figure 11: Frequency measurement results for the unstable cut.

5.2.2 Insert nose radius effects on chatter limit

In order to verify the stability model for insert nose radius, and its effects on the absolute stability limit chatter experiments were conducted using inserts with different nose radii (Figure 8.a-c) and with conditions summarized in section 5.1. 10° of side edge cutting angle, 5° of rake angle, and 5° of inclination angle are used during the tests.

As discussed in section 3.1 eqn. 30. is solved in order to obtain the absolute stability limit sweeping the chatter frequency around the tools most flexible mode, ie. bending mode in this case. Number of elements for nose region, used during simulation tests were 15, 30, and

45 for inserts having 0.4, 0.8 and 1.2 mm nose radiuses.

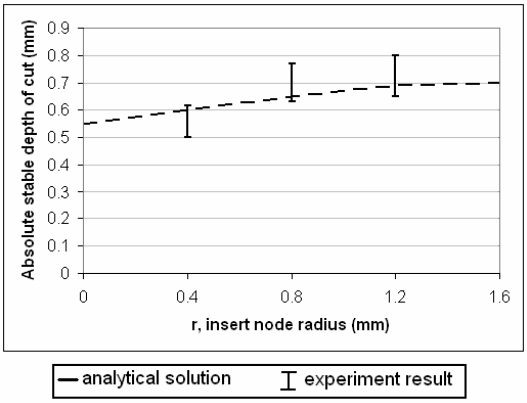

Figure 12: Chatter test results for inserts having different nose radiuses.

In the experiments, the tool was much more flexible than the workpiece, so the dynamics of the process was dominated by the tool. The side cutting edge angle was relatively small, thus the effect of the nose radius on the stability is expected to be small (as discussed in section 4.3.).The experimental results for different nose radii are shown in Figure 12. The chatter tests were repeated several times, and the experimental data ranges in Figure 12 represent variation of the stable depths observed in the experiments. Overall, there is an increase in the absolute stability limit with the nose radii. This is expected as the increase in the nose radius reduces the effect of tool flexibility. The predicted stability limits and experimental results show reasonable agreement.

6 CONCLUSIONS

The main achievements of the current study can be summarized as follows:

•An analytical stability model for turning considering tool and workpiece dynamics in a multi dimensional manner is formulated

•The proposed analytical model includes the important parameters in the turning geometry, i.e. practical tool angles, and nose radius.

•A solution procedure is developed for stability limit with the proposed elemental model for the insert nose.

•The effect of important process parameters on the stability are demonstrated using simulations based on the model

•The proposed analytical solutions are verified by experiments

7 REFERENCES

[1] Tlusty, J., Polacek, M. “The Stability of Machine Tools Against Self Excited Vibrations in Machining”, *Int. Research in Production Engineering*, ASME, 465-474, 1963.

[2]Tobias, S.A. and Fishwick, W., 1958, The Chatter of Lathe Tools Under Orthogonal Cutting Conditions, Trans. of ASME, 80:1079-1088

[3] Minis, I., and Yanushevsky, T., 1993, A New Theoretical Approach for the prediction of the Machine Tool Chatter in Milling, ASME J. Eng. Incl., 115, pp.1-8.

[4] Budak, E., and Altintas, Y., 1998, Analytical Prediction of Chatter Stability in Milling-Part I: General Formulation; Part II: Application to Common Milling Systems, ASME J. Dyn. Syst., Meas., Control, 120, pp. 22–36

[5] Rao, C. B., Shin, Y. C., “A Comprehensive Dynamic Cutting Force Model for Chatter Prediction in Turning”, *International J. of Machine Tools&Manufacture* , Vol. 39, 1631-1654, 1999.

[6] Budak, E., Altintas, Y, “Analytical Prediction of Chatter Satbility in Milling – Part I: General Formulation”, *Transactions of the ASME* , Vol. 120, 22-30,March 1998.

[7] Clancy, B.E., Shin, Y.C., “A Comprehensive Chatter Prediction Model for Face Turning Operation Including Tool Wear Effect”, *Int. J. of Machine T.&M.*, Vol. 42, 1035-1044, 2002.

[8] Atabey, F., Lazoglu, I., Altintas, Y., “Mechanics of Boring Processes – Part I”, *Int. J. of Machine T.&M.*, Vol. 43, 463-476, 2003.

[9] Lazoglu, I., Atabey, F., Altintas, Y., “Dynamic of Boring Processes: Part III – Time Domain”, *International Journal of Machine Tools&Manufacture*, Vol. 42, 1567-1576, 2002.

[10] Ozdoganlar, O. B., and Endres, W. J., 2000, “An Analytical Representation of Chip Area for Corner-Radiused Tools Under Depth-of-Cut and Feed Variations,” *ASME J. Mfg. Sci and Engg.*, 122, 660-665, 2000.

[11] Armarego, E.J.A., Brown, R.H., *“The Machining of Metals”*, Prentice-Hall, 1969.

[12] Armarego, E.J.A. and Whitfield, R.C. (1985). Computer based modeling of popular machining operations for force and power predictions. *Annals of the CIRP*, 34: 65-69)

[13] Budak, E., Altintas, Y. and Armarego, E.J.A. (1996). Prediction of milling force coefficients from orthogonal cutting data. *Trans. ASME J. of Man. Sci. and Eng.*, 118: 216-224.

[14] Altintas, Y., *“Manufacturing Automation”*, Cambridge University Press , 2000.

[15] Altintas, Y. and Budak, E, “Analytical prediction of stability lobes in milling”, *Annals of the CIRP*, 44: 357-362

[16] *http://www.malinc.com :Cutpro® website.*